Reversing entropy: deblending and imaging physical modeling data

David C. Henley and Joe Wong

ABSTRACT

Physical modeling has become one of the key activities pursued by students and staff at CREWES. It is an important technology for verifying the theory of elastic wave propagation, as well as for developing and testing acquisition and processing techniques which are applicable to full scale field seismic operations. Many of the problems which afflict full-scale seismic exploration are present in the physical modeling environment as well. One of these, the time required to acquire a massive 3D seismic survey, has found a partial solution in the use of multiple simultaneous sources during the field acquisition. Here, we analyze a small portion of a large 3D data set acquired in the CREWES physical modeling facility using 8 simultaneous sources (to decrease acquisition time by a factor of 8). We show that with suitable acquisition geometry, the simultaneously acquired source records can be untangled or 'deblended' and subsequently imaged with no significant crosstalk from the simultaneous sources. While this achievement in itself is not unique, we demonstrate a new implementation based on previous wavefield separation work. We document here our increasingly sophisticated ability to acquire and process complex physical model data in a way that emulates actual field seismic surveys.

INTRODUCTION

One of the continuing trends in exploration geophysics is the increase in the sheer physical size of field surveys. Not only are the actual physical dimensions on the earth's surface increasing, but the number of source points and receiver stations continues to increase, as well, in pursuit of unaliased sampling, not only of subsurface structure, but also, mainly on land, the organized surface noise that contaminates much seismic data. As the size and resolution increases, so does the effort and cost; so various methods have been devised to help reduce cost while acquiring the massive volumes of seismic data. One of the more prominent methods is to use multiple simultaneous sources recorded into a full spread or patch of surface sensors. For marine surveys, airguns or airgun arrays are the sources most often deployed simultaneously, while on land the source of choice is Vibroseis. If the sources are separated sufficiently on the surface, or differ in output characteristics, the wavefields due to each source can be separated from the full recorded wavefield by processing techniques generically called 'deblending' before entering a conventional processing stream for imaging.

While there are several signal processing concepts that can be used to disentangle signals transmitted simultaneously into a common medium (for example: Beasley, 2008; Cheng and Sacchi, 2013; and Trad et al, 2012), we investigate here one of the simpler and more widely used methods: physical separation of the sources coupled with wavefield-separation processing. Because the outgoing wavefield from each source, and the associated backscatter, travel at specific velocities in the earth, as dictated by the earth materials and their geometrical structure, each mode of wave propagation from a particular source exhibits a pattern of coherence across the array of receivers that is

unique to the physical location of the source. As long as individual sources are sufficiently far apart, their wavefield coherence patterns will differ enough to allow them to be separated by various processing algorithms. A seismic trace 'supergather' consisting of many individual traces, on which the wavefields of several sources have been recorded simultaneously, can hence be decomposed and expanded into individual source gathers by applying wavefield-separation techniques to the supergather, once for each source, with the separation geometry parameters adjusted to the unique coordinates of each source. Thus, a supergather consisting of N traces, recording a wavefield from n simultaneous sources can be separated into n unique gathers of N traces each, by applying the wavefield separation n times to the original gather, changing the source origin coordinates for each pass.

There are several related aspects of acquisition and deblending to be examined in relation to this physical modeling study:

- Constructing an effective wavefield-separation processing flow and observing its relative effectiveness at various stages of processing.
- Estimating the minimum source separation that can be used for this technique to remain effective.
- Estimating the maximum receiver separation that can be used for this technique.
- Observing the separation effectiveness as a function of survey geometry (offset of source line from receiver line, for example).

The data set used for testing deblending was acquired mainly for the purposes of studying imaging and other interpretive processing on a complex model simulating buried channels and puck-shaped zones of anisotropy (Wong, 2013a). It was quite large and required a very significant amount of time and effort to generate, even using simultaneous sources. Hence the survey was performed only once, and the above questions were studied by analyzing and observing the existing survey and its characteristics, not by repeating the survey with varying parameters. The resulting guidelines pertaining to geometrical parameters are accordingly heuristic, but instructive, nevertheless.

THE EXPERIMENT

The actual physical model for which we developed and tested our deblending scheme was described in detail by Wong (2013a), and is shown in Figure 1. The areal coverage map for source and receiver positions is shown in Figure 2. For our deblending test, we used only a small portion (1/16) of the complete data set, selectively covering one corner of the complete physical model. While this small subset of the complete survey does not contain enough data to satisfactorily image, in 3D, one of the target anisotropic 'pucks' in the model, it can be used to judge the effectiveness of deblending, and various 2D CMP stacks can be formed within this data set to help with this evaluation. The primary reason for choosing this data set for our evaluation is that it is small enough to process quickly,

yet large enough to give us a feel for processing the entire survey. Because of its compact size, the data volume allowed many trial processing runs in the course of our work.

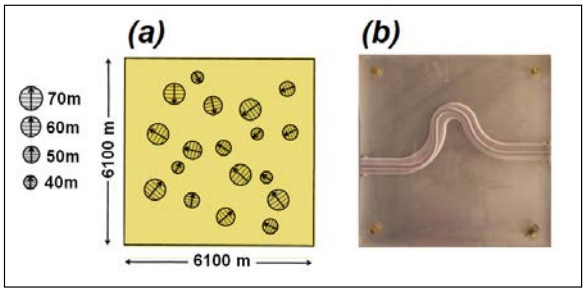

Plan view of physical model target layers

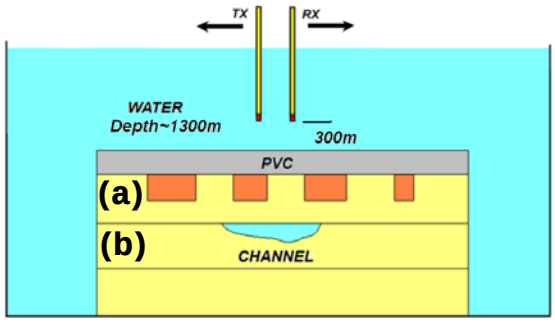

Cross section of physical model target layers

FIG 1. Details of the physical model. Upper panel shows the target layers (random HTI pucks and sinuous channel) in plan view; lower panel shows layers in cross section.

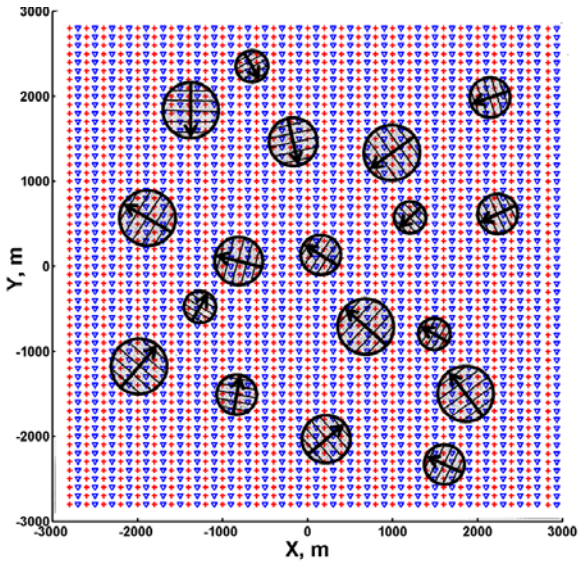

Acquisition geometry for physical model relative to 'puck' layer

FIG 2. Plan view of the acquisition geometry layout for the physical model.

The acquisition was performed as a marine survey, with both sources and receiver deeply submerged beneath the surface of a layer of water covering the solid physical model, as described in Wong (2013a). The depth of immersion was sufficient to eliminate the interference of both source and receiver ghosts. A source array was constructed, consisting of 8 piezopin transducers, each separated from its nearest neighbors by 4 source intervals (400m scaled distance). A single piezopin served as a receiver; and it occupied, in succession, each of 112 receiver positions 50m apart along a receiver line, parallel to the source line. The source array was initially positioned at the beginning of the first source line, at the edge of the model, and fired repeatedly until each receiver position had been recorded for the first receiver line. After all 112 stations in a receiver line were recorded (forming an eight-source supergather), the starting position of the receiver piezopin was incremented by 100m scaled distance *perpendicular* to the source array, to begin the next receiver line, and the acquisition was repeated for all 112 positions on the new receiver line, *with no movement of the source array*.

When 56 receiver lines had been recorded, spaced 100m (scaled distance) apart, the source array was moved 100m along the source line, the receiver piezopin was moved back to its original starting position on receiver line 1, and another 56 receiver lines were recorded. By incrementing the source array position by 100m for each group of 56 receiver lines, four passes of 56 receiver lines provided coverage for a patch defined by 32 sources spaced 100m apart along the edge of the survey, recorded by a 56x112 array of receivers, distributed over the entire upper surface of the model. The source array only occupied half of the initial source line along one edge of the model for the subset of data we consider here, so the resulting 3D subsurface coverage for this patch was quite asymmetric, particularly in the population of azimuths. Hence, our image analysis of deblending will only use 2D displays of trace gathers and 2D CMP stacks along inline and crossline directions through the incomplete data set.

The survey for the entire model was completed as follows: after acquiring the patch corresponding to the first half of the source line, the source array was moved along this source line to the first position in the second half of the source line. Each of the 56 receiver lines was recorded using this source array position, then the source array moved 100m inline, and another 56 receiver lines recorded, etc. Upon completion of the first source line data subset, the source array was positioned at the beginning of the second source line, parallel to the first source line, but 100m inside the edge of the model. Acquisition of the data supergathers for the second source line for the complete 56x112 receiver array then proceeded exactly as described above for source line 1. Data for each of the 56 source lines were recorded in exactly the same way, resulting in a set of supergathers corresponding to an array of 56x56 sources fired 8 at a time into a receiver array 56x112. This complete data set has been described in Wong (2013a), and its preliminary analysis in Wong (2013b).

Raw data analysis

To give some feel for the geometrical problems involved in acquiring and deblending a seismic survey like the model experiment described above, we first consider some raw

data 'supergathers' for selected receiver lines within the survey. Figure 3 shows the supergather acquired for receiver line 1 when the source array is in its starting position at the beginning of source line 1. The direct water wave is very evident on this trace gather, since its moveout is nearly linear with offset. The moveout would be strictly linear, if the source and receiver lines were coincident; but this is impossible because of the lateral dimensions of the piezopin transducers. Nevertheless, the water wave event created by each of the individual sources seems easy to separate from all the others, at least by eye. Deeper events, though they have distinct apexes, each related to source position, seem less obviously separable. The gather in Figure 3 has been subjected to AGC in order to keep all the events relatively visible, but there are large amplitude disparities in the underlying data. Most notably, the direct water wave is the strongest event by far on this supergather, as well as being the slowest, and the most highly aliased spatially. Deblending parameters will necessarily be strongly influenced by this event and its characteristics, since the removal of its interference from neighboring source gathers is crucial.

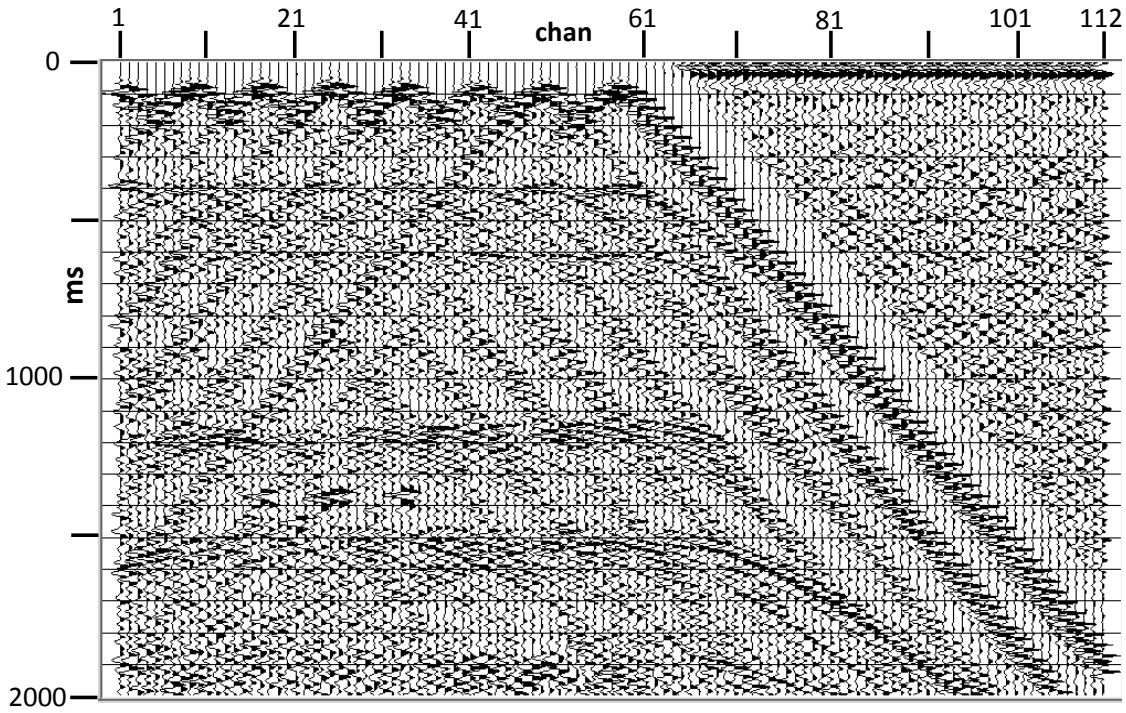

FIG 3. 'Supergather' acquired using receiver line 1 and the 8-source array positioned at the beginning of source line 1. Direct water arrivals are nearly linear.

When the decision is made to use multiple simultaneous sources to speed acquisition, two key acquisition parameters must be chosen prior to the experiment: the number of sources, and their spacing. While the number of sources, at least in a field setting, is usually dictated by logistics, their spacing must be chosen using other considerations. Referring to Figure 3, it is obvious that if the sources were spaced 120 stations apart, their wavefields would never interfere for the entire chosen recording time of 2000ms. For this survey, that restriction is unworkable, since the survey area itself is only 112 stations

wide. At the other extreme, if the source spacing were only one station, the wavelength of the various event arrivals would ensure that the wavefields from adjacent sources are too entangled to separate, since their waveforms would be overlapped and superimposed. Furthermore, the amplitude of an event for a selected source would not be much stronger than that of the same event due to neighboring sources, providing little discriminating power. Intuitively, the minimum source separation appears to be the one for which waveforms for the same event on different source wavefields do not significantly overlap visibly in time, except near the apex of their hyperbolae. Using this heuristic guideline on the supergather in Figure 3, we see that when the source separation is 4 shot stations, the direct water wave shows little overlap of waveforms, and the 400ms reflection appears well-separated as well. Deeper events (1200ms and 1500ms, for example) show significant overlap on several traces near the apexes of the respective event hyperbolae. We interpret this to mean that the chosen source separation of 4 source stations is likely adequate for shallow events, but marginal for deeper ones, in terms of effective deblending.

At first glance, removal of the water wave from the supergather seems to pose a particular problem, since the wave is seriously aliased everywhere, as is the reflection event from the shallowest reflector at about 400ms. For most wavefield separation or coherence noise attenuation techniques to work properly, aliasing of the events targeted for removal must be minimal (Henley 2003); in this case suggesting that the receiver spacing during acquisition should have been ½ or even ¼ of the spacing actually used. This would, of course, have meant an acquisition time of twice or four times the actual acquisition time—an unacceptable alternative, given that using simultaneous sources to *reduce acquisition time* was one of the goals of this modeling work.

Figure 4 shows the scaled source spectrum for the piezopin transducer, while Figure 5 shows the supergather of Figure 3 when bandlimited to approximately ¼ of the original source bandwidth in order to reduce aliasing (an alternative to decreasing receiver spacing). Clearly, too much meaningful detail is sacrificed to consider this a viable option. Fortunately, as shown by Henley and Wong (2011a, 2011b) and Henley et al (2013a, 2013b), there are processing alternatives that provide one path out of the dilemma.

FIG. 4. Scaled source spectrum for the piezopin transducers used in the source array for surveying the physical model.

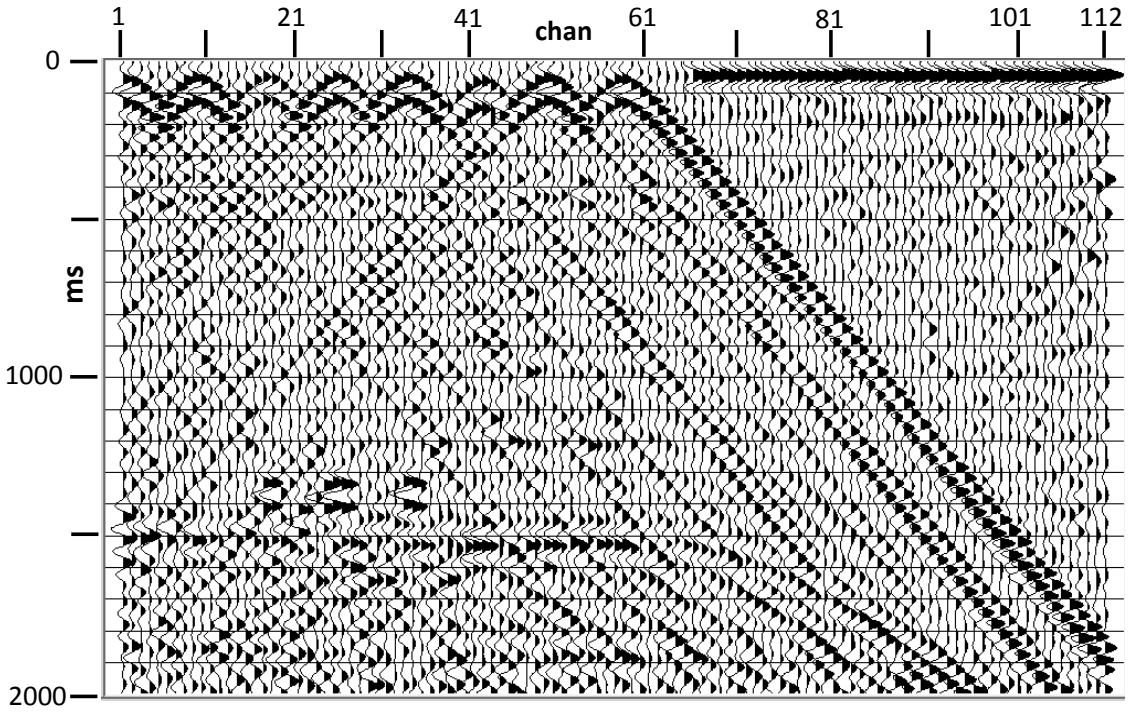

FIG. 5. Supergather from Figure 3 after bandlimiting to reduce spatial aliasing due to receiver spacing. Clearly, too much detail is sacrificed by this alternative.

At this point in the processing of a supergather, our goal is the preservation of all coherent signal from a *single source*, for each of the eight sources in turn, rejecting all other coherent energy as noise. For this purpose, we consider the direct water arrival to

be part of the coherent wavefield for an individual source to be preserved by deblending—only at a later stage of processing will we consider it an undesirable noise to be removed from the source gather.

For purposes of illustration, we look at two more supergathers, one for receiver line 25 (parallel to the source line, but midway across the model surface), and one for receiver line 50 (parallel to the source line, but near the far edge of the model surface). Figure 6 shows the supergather for receiver line 25. The direct water wave is now a broadside wavefront, with obvious hyperbolic moveout, referenced to each source location. While aliasing is somewhat less, so is the apparent event separation near the apex of each hyperbola, compared with Figure 3. Deeper events, or reflections, are affected even more by this 'broadside' geometric configuration, also becoming less separable. Figure 7 shows the supergather for receiver line 50; and the only event visible, because of the obliquity of the angle and recording time limit, is the direct water wave. The distinct hyperbolae are even less separable for this receiver line than for receiver line 25—but there are no reflections on this supergather, in any case, due to the extreme source-receiver offsets involved, and the recording time limitations.

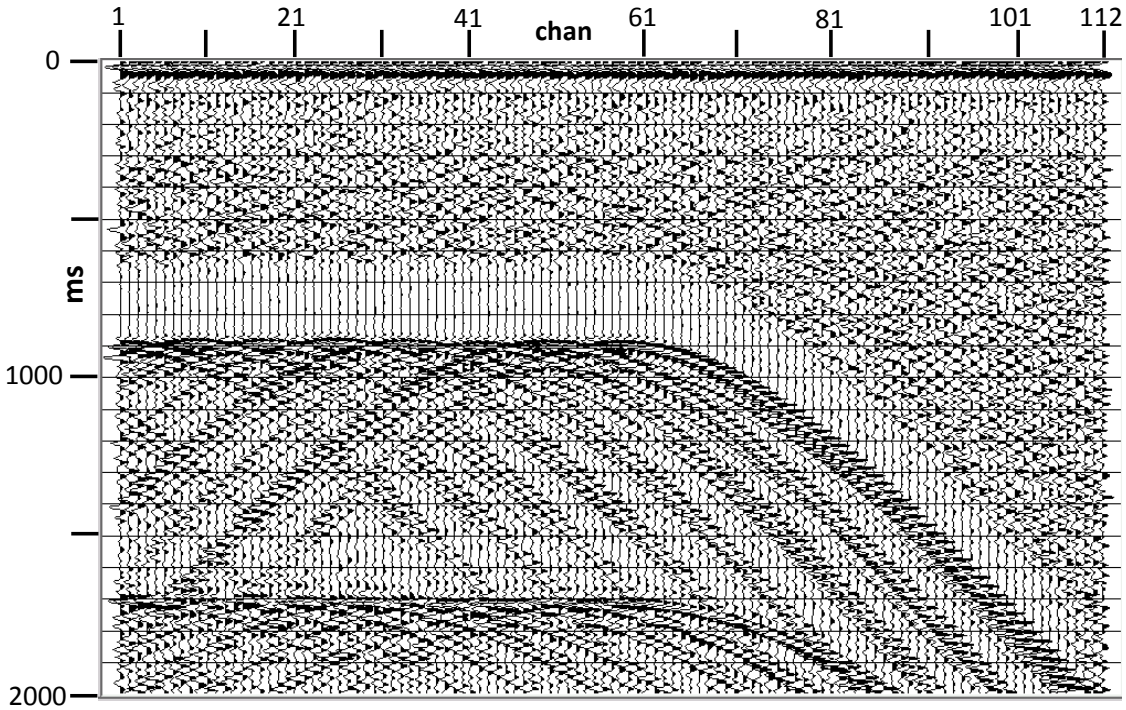

FIG. 6. Supergather for receiver line 25 for the source array in the starting position at the beginning of source line 1. Direct water arrivals are visibly hyperbolic.

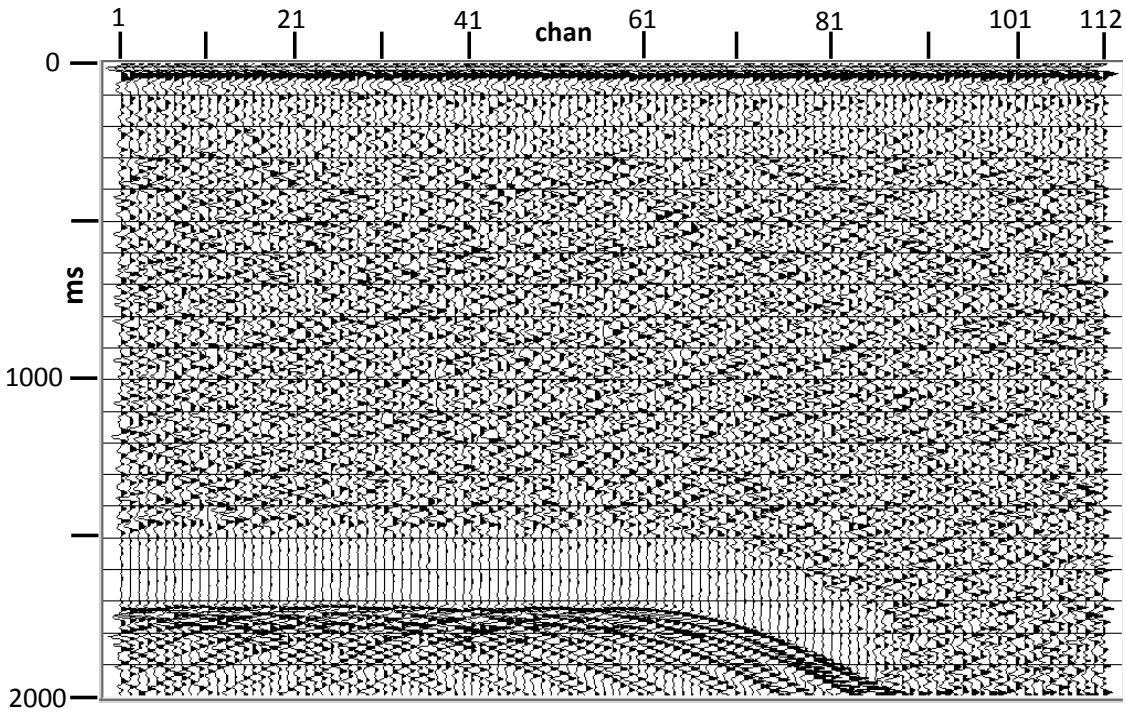

FIG. 7. Supergather for receiver line 50 for the source array in the starting position at the beginning of source line 1. Direct water arrivals are the only coherent energy visible.

Deblending analysis

To begin any deblending operation, it is necessary to associate proper coordinates with each source contributing to a particular supergather, since it is these coordinates which select the particular source whose response is to be extracted from a supergather and which thus control the application of the wavefield separation. From the master coordinate system for the entire survey, source coordinates can be computed (on the supergather, only sou_x is legitimate, while sou_y is indeterminate). Then, since each deblended source gather requires its own unique set of source-receiver offsets, these must be computed from the new source coordinates and the existing receiver coordinates. It is important to properly reconstruct the sign of the offset, as well, relative to the nearest-offset receiver for each source position, since this is required for geometric remapping operations in the 2D data plane (Henley and Wong, 2013a).

If we examine the supergather in Figure 3 once again, we can see that the wavefield for any particular source does not extend to shallower times or greater offsets than those defined by the direct water wave arrivals for that source. Hence, the first deblending operation could be a simple muting operation, unique to each source position, discarding data samples outside the water-arrival cone. This would certainly eliminate any coherent energy from nearby sources—but it would have no effect on events from nearby sources falling within the water-arrival cone for a particular source. Another operation to consider, however, is the normal moveout operation. When defined by a moveout velocity function which begins with the water velocity, the NMO operation not only flattens the events whose velocities are represented, but it discards samples above the water-arrival cone, and also removes the aliasing from the water arrivals and any other

events with velocities properly represented in the operation. Furthermore, if stretch limits are removed, the NMO operation can be reversed exactly for the data within the water-arrival cone. Another attractive feature of this operation is that the moveout velocities need not be known exactly in order to de-alias the events and approximately flatten them for removal of interfering events. They can, in fact, be estimated well enough by using the velocity fitting tool in the Trace Display operation in ProMAX.

Figures 8, 9, 10, and 11 are examples of partially deblended source gathers resulting from simply supplying the correct source geometry and applying NMO using estimated velocities. Figures 8 and 9 are gathers corresponding to source position number 1 at receiver line 1 and 25, respectively. Interestingly, the water wave event is so stretched on these gathers that it could be nearly eliminated with just a bandpass filter. The first reflection, at 400ms, on the other hand, is still recognizable on both gathers. While hints of other flattened events are visible on these gathers, it is obvious that much of the coherent energy consists of steeply-dipping events that represent the interfering wavefields from adjacent sources. Figures 10 and 11 show the corresponding partially deblended gathers for a source position further along the source line, recorded into receiver lines 1 and 25. As before, the water wave event is greatly distorted by stretch, the 400ms reflection is easily recognized, and other flattened events have become more evident on these two gathers.

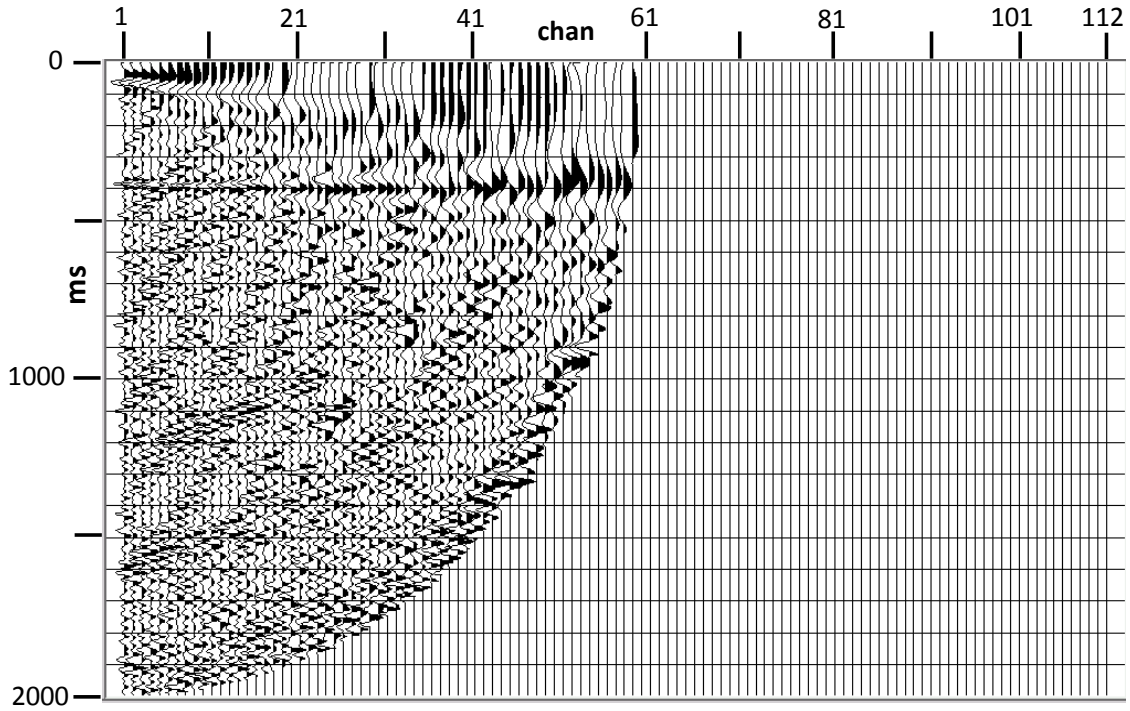

FIG. 8. First step in deblending supergather from initial source array position into receiver line 1. Selected source position is no. 1 in the 8-source array.

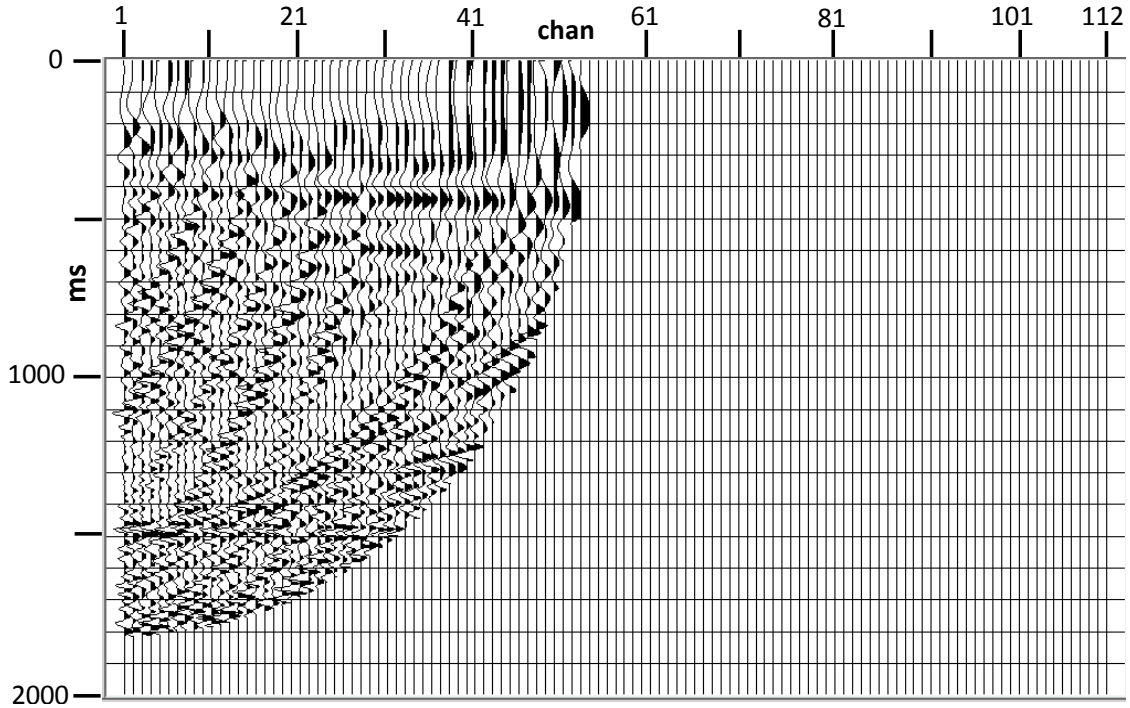

FIG. 9. First step in deblending, source no. 1, receiver line 25. Most visible coherent energy is interference from neighboring sources in the array.

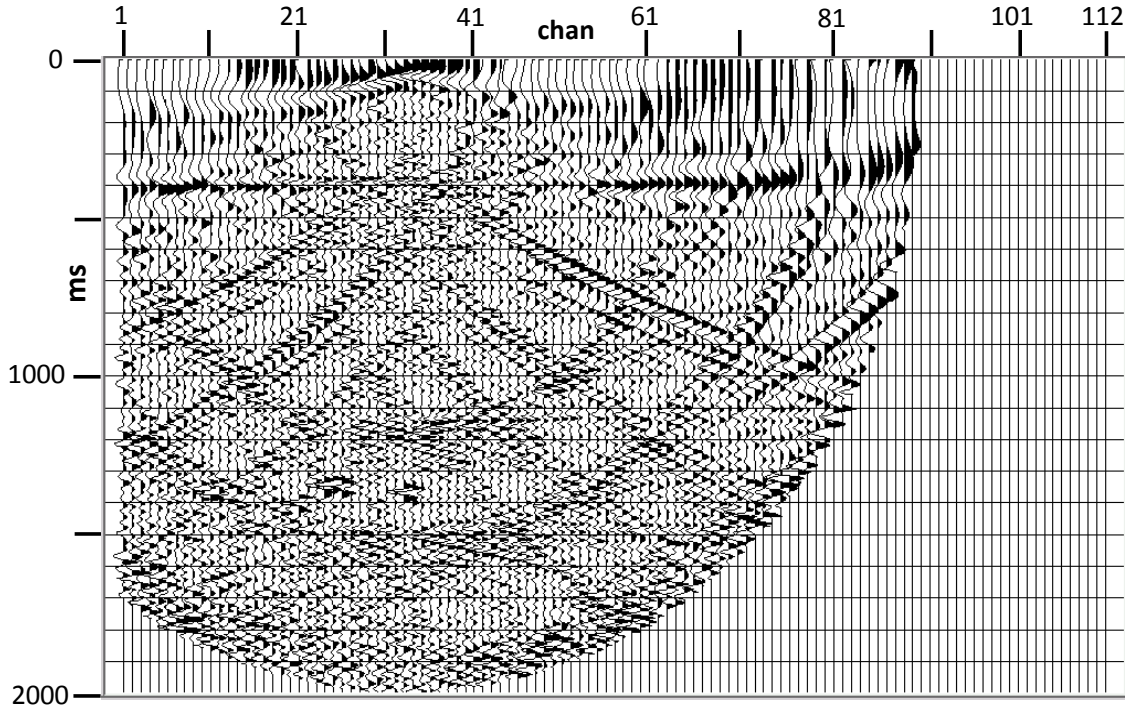

FIG. 10. First step in deblending, source position no. 17, receiver line 1.

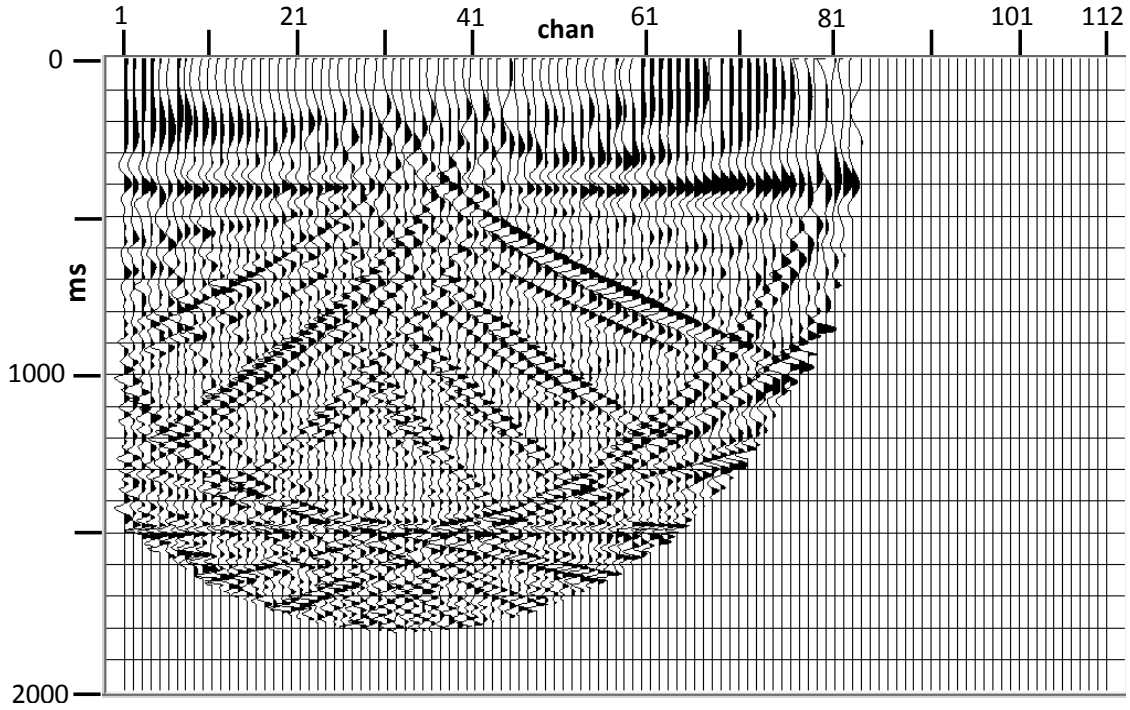

FIG. 11. First step in deblending, source position no. 17, receiver line 25.

With source gathers as displayed in Figures 8, 9, 10, and 11, we can measure the dips (apparent velocities) of all non-flat events, knowing that they are interfering wavefield components from neighboring source positions. Interestingly, because of the overall flattening of the desired wavefield events, and the stretch applied to everything, little aliasing is apparent, even on the interfering events, which bodes well for efficient estimation and subtraction of these events using RT dip-filtering techniques (Henley, 2011b; Henley and Mahmoudian, 2013b). When we measured all visible dipping events and designed RT dip filters to remove them, the corresponding source gathers were as shown in Figures 12, 13, 14, and 15. When comparing these figures with Figures 8, 9, 10, and 11, respectively, it can be seen that nearly all of the non-horizontal energy has been removed.

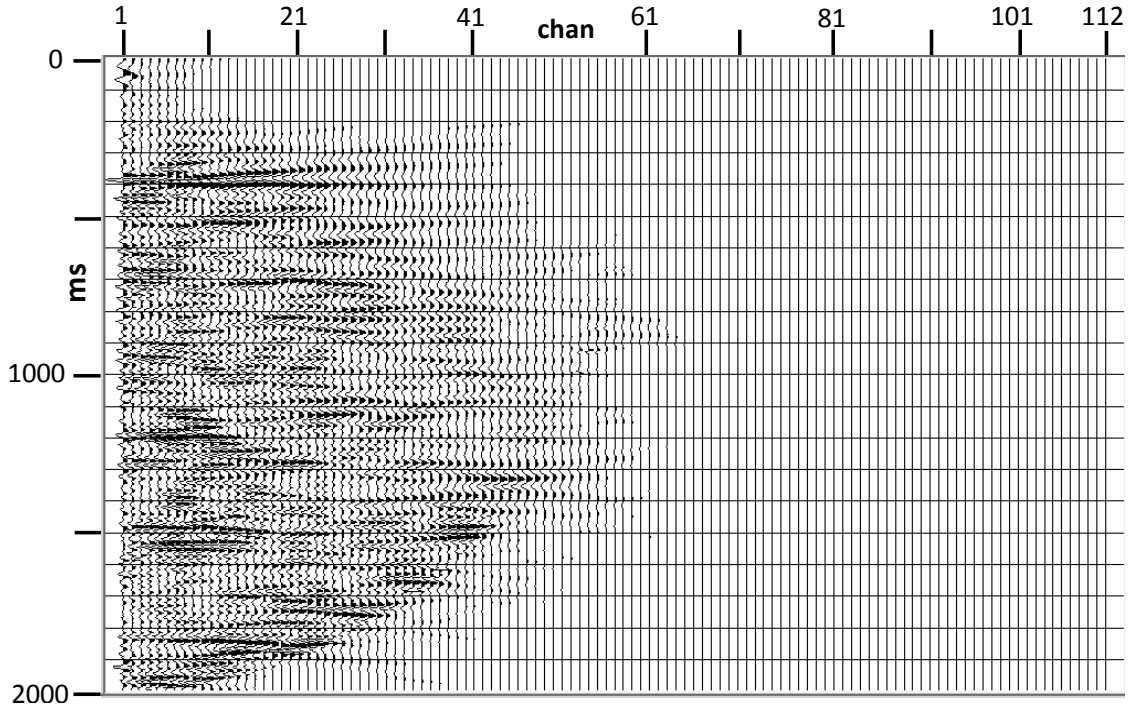

FIG. 12. Second step in deblending; RT dip filters eliminate non-horizontal events, source no. 1, receiver line 1. Compare with Figure 8.

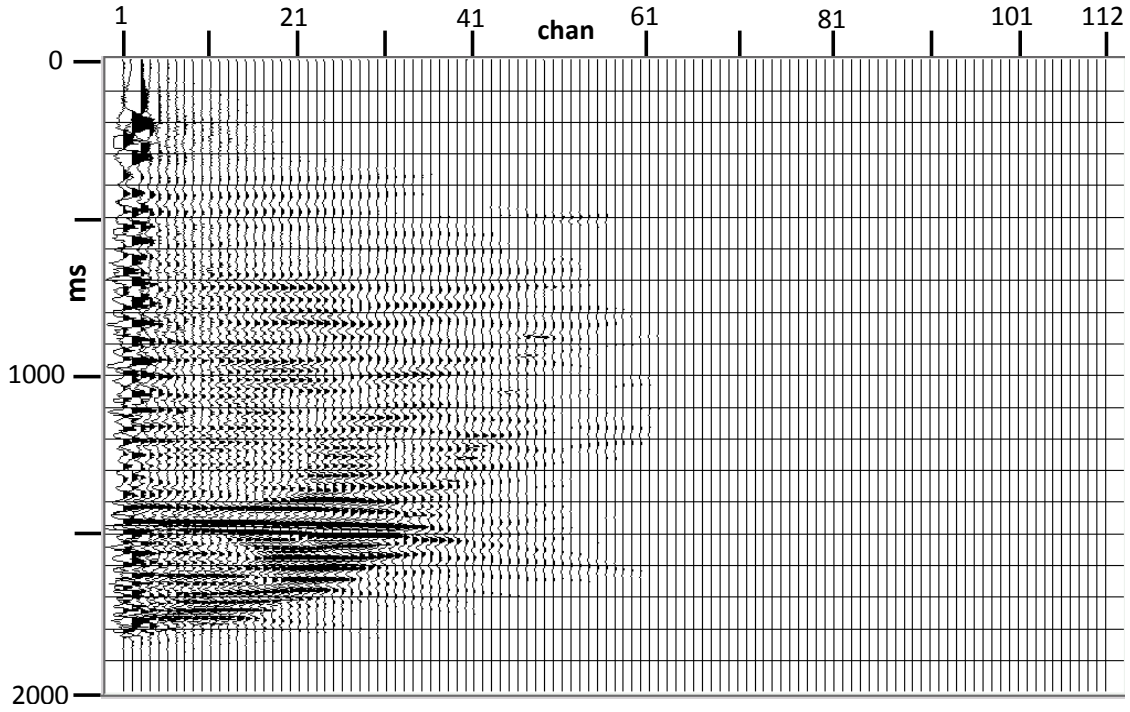

FIG. 13. Second step in deblending; RT dip filters eliminate non-horizontal events, source no. 1, receiver line 25.

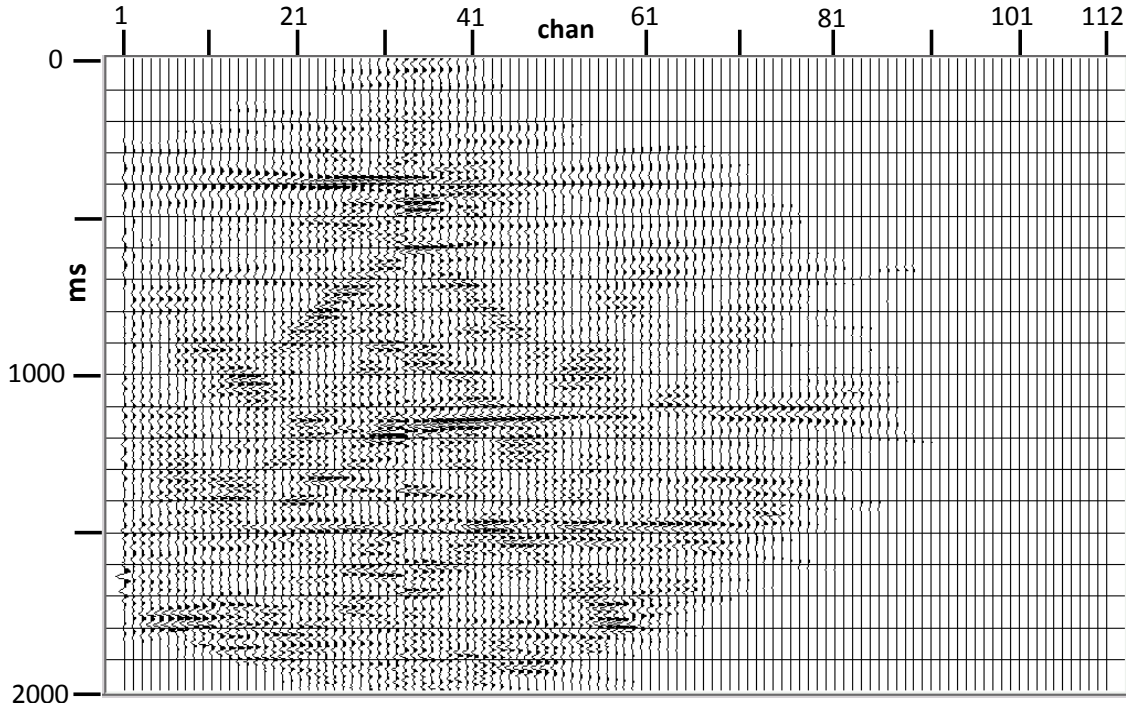

FIG. 14. Second step in deblending; RT dip filters eliminate non-horizontal events, source no. 17, receiver line 1. Some aliased residual events can still be seen.

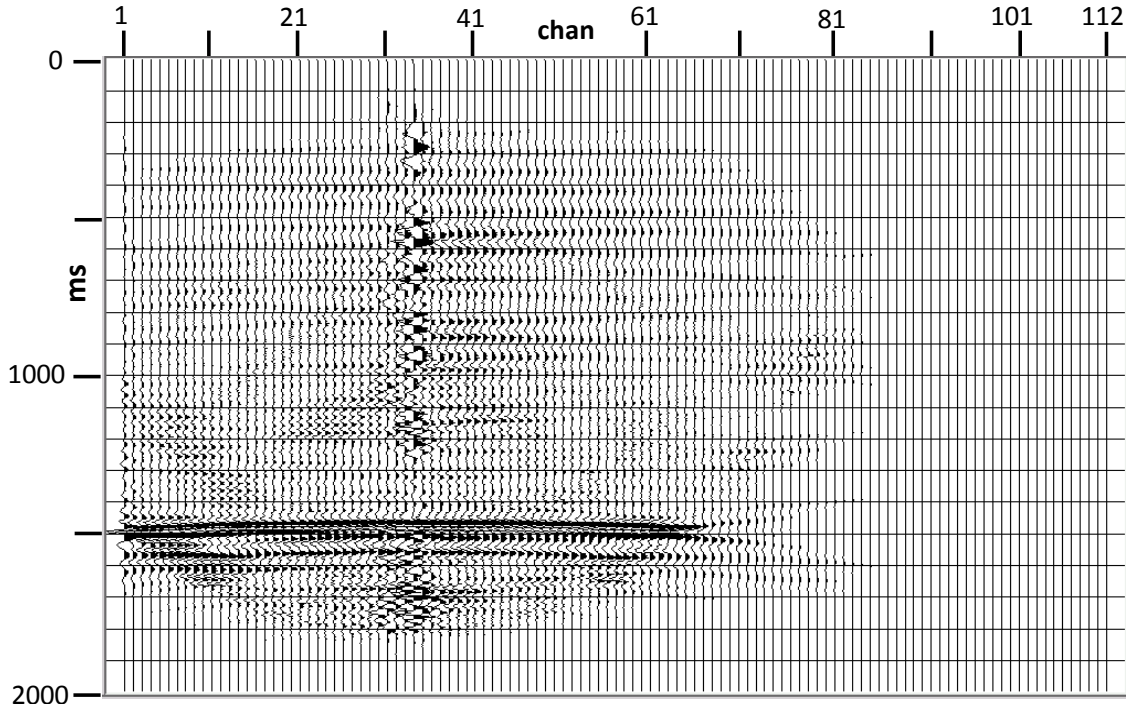

FIG. 15. Second step in deblending; RT dip filters eliminate non-horizontal events, source no. 17, receiver line 25.

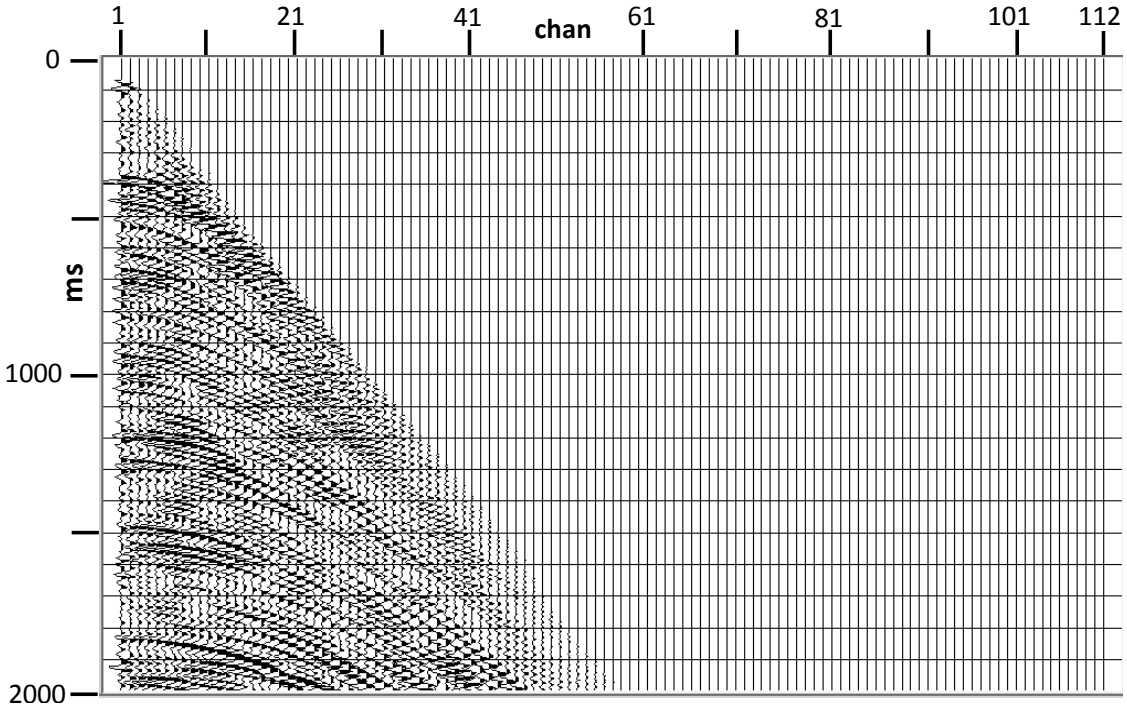

FIG. 16. Deblending completed for source position no. 1, receiver line 1.

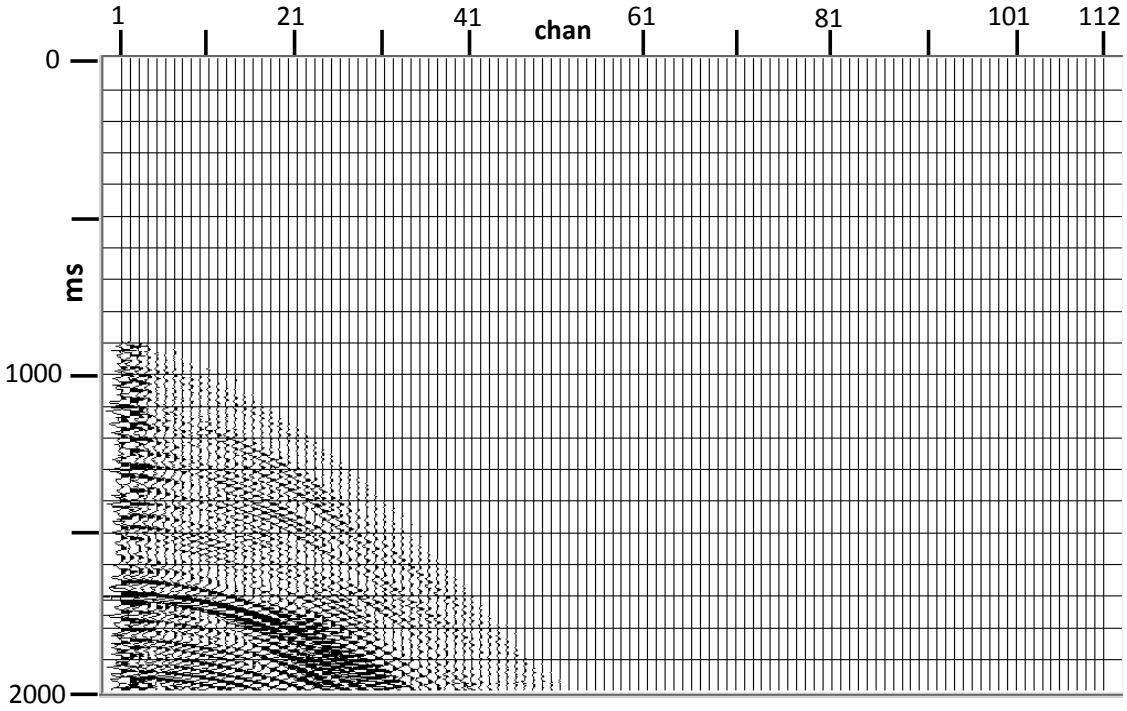

FIG. 17. Deblending completed for source no. 1, receiver line 25.

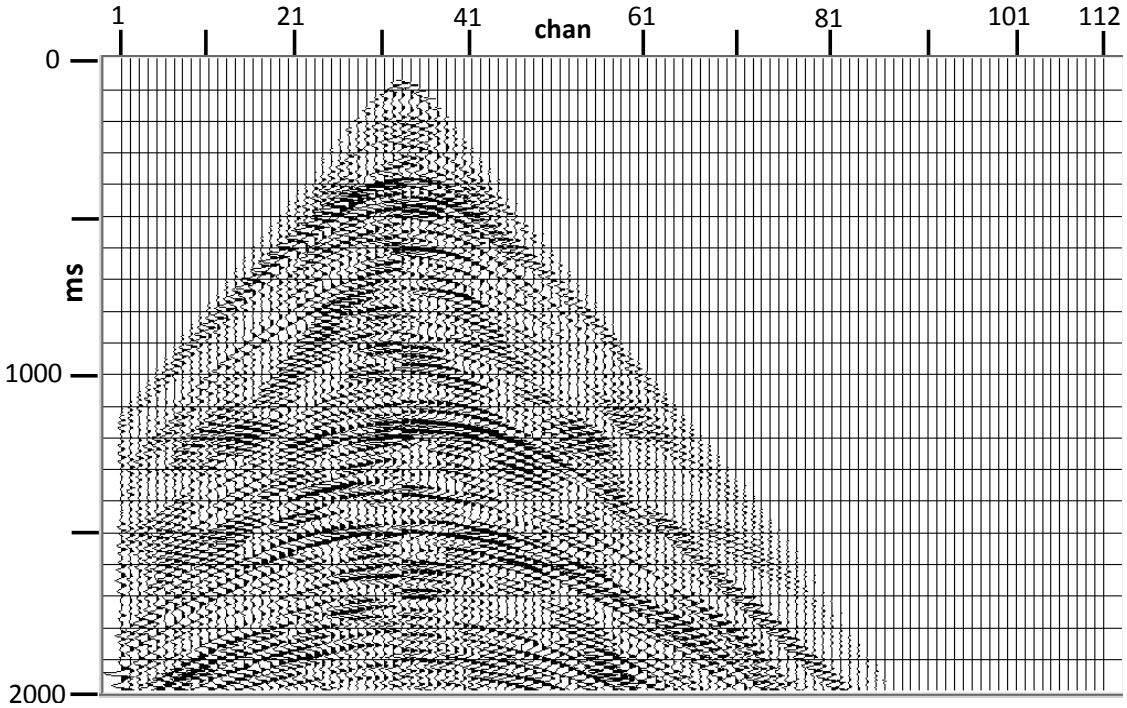

FIG. 18. Deblending completed for source no. 17, receiver line 1.

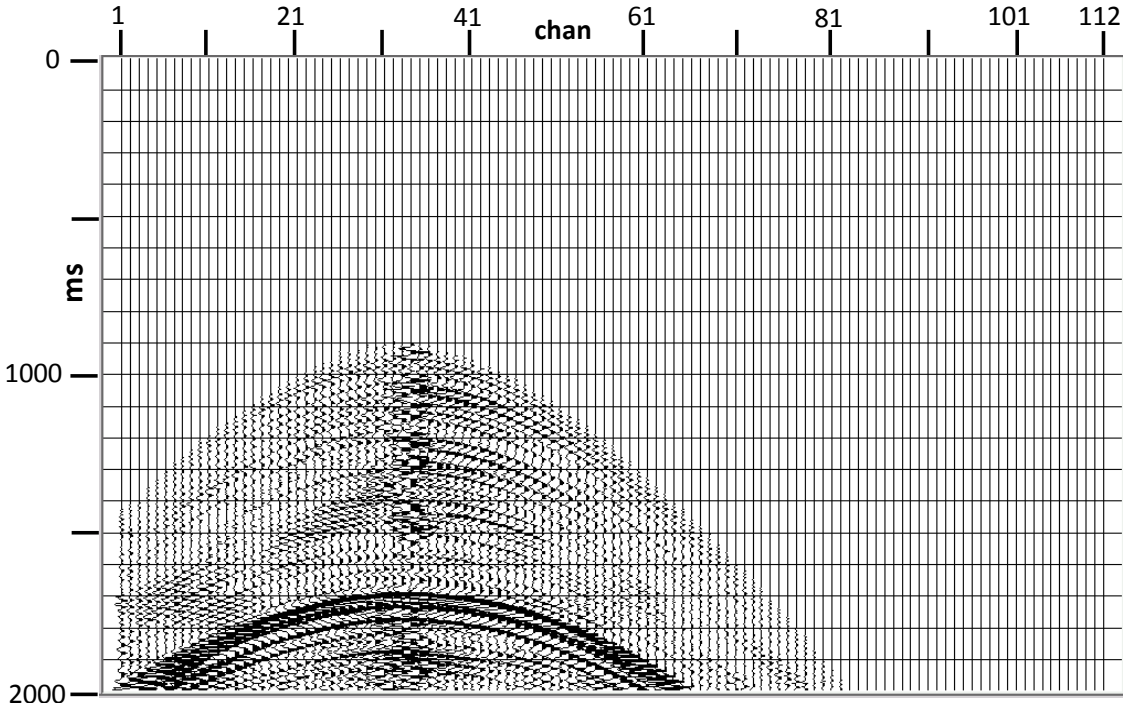

FIG. 19. Deblending completed for source no. 17, receiver line 25.

The final step in deblending is to restore the NMO to all the deblended gathers, since the moveout velocities used for the deblending operation are estimates made from analysis of the noisy supergathers. More precise moveout velocity estimates can be made

from the deblended source gathers and used for purposes of CMP stacking and other imaging operations. The fully deblended source gathers for source positions 1 and 17, for receiver lines 1 and 25 are shown in Figures 16, 17, 18, and 19. They were extracted from the supergathers first shown in Figures 3 and 6. We show these supergathers again in Figures 20 and 21, with the extracted source gathers outlined for comparison with Figures 16, 17, 18, and 19. It is clear from this comparison that the wavefield separation is nearly complete for the extracted source gathers, and that they can now be processed like ordinary source gathers.

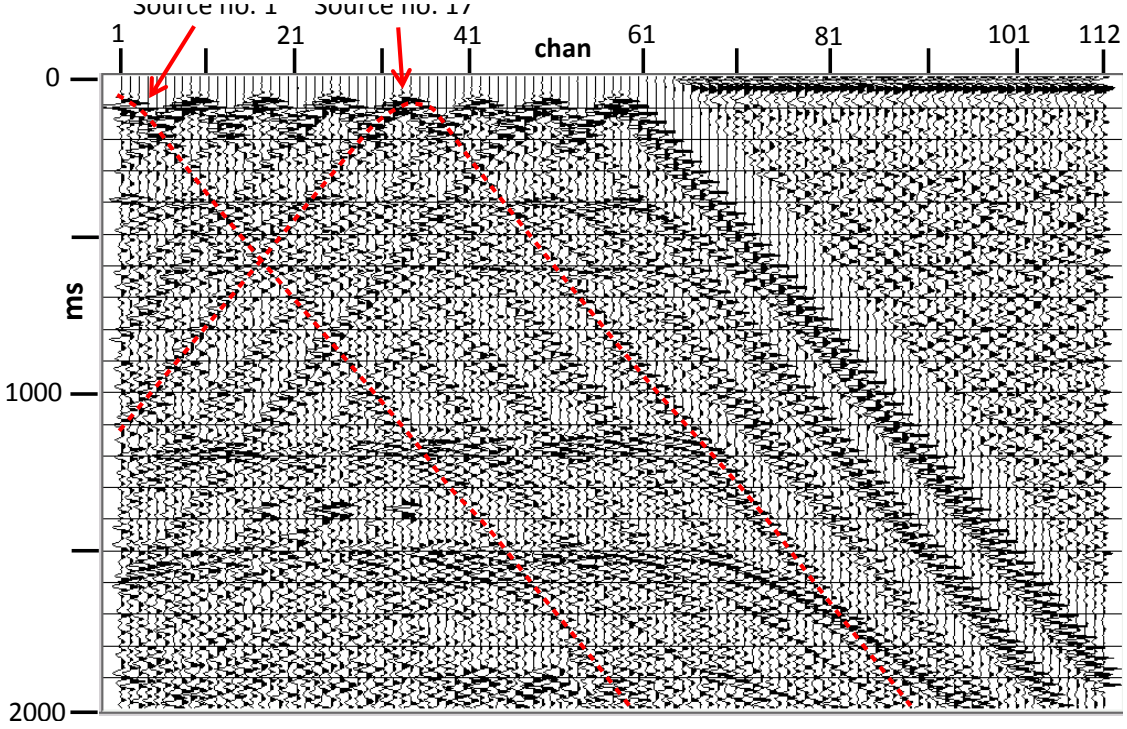

FIG. 20. Original supergather from Figure 3, with the outlines of the two extracted source gathers shown in Figures 16, and 18, respectively.

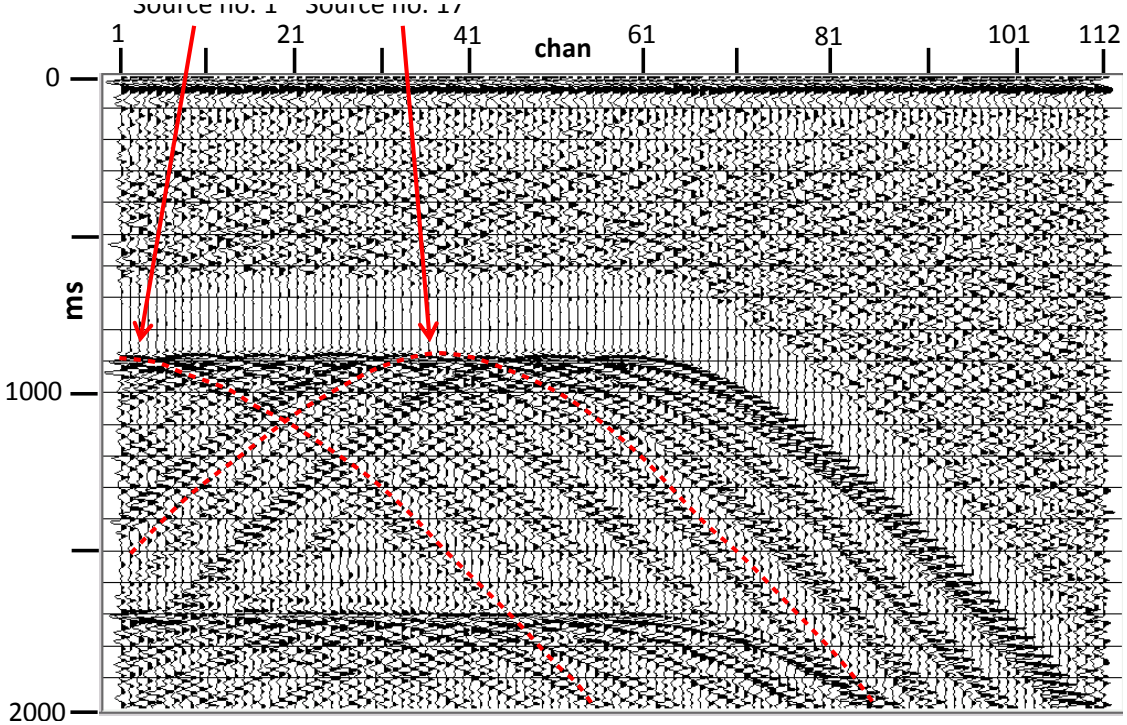

FIG. 21 Original supergather from Figure 6, with the outlines of the two extracted source gathers shown in Figures 17 and 19, respectively.

It should be noted that since we used eight simultaneous sources to acquire these data, each supergather must be processed eight times, once for each individual source, since the trace headers carrying the source geometry information must be set for each source individually in order to properly deblend that particular source gather from the supergather.

Considering the particular shooting plan that was executed to acquire the data set (moving the source array incrementally along each source line to record a full set of receiver lines, then moving to the next source line), The easiest way to plan the deblending process for the entire 3D survey is probably to divide the completed survey into 56 files, each of which contains all the data recorded using one source line. The benefit in doing this is that for each file of data, the sou_x trace header can remain constant, requiring computation of only the sou_y coordinate for each source, and the assigning of a unique ‘source’ trace header for each source position. Using the source and receiver coordinate headers for each source and receiver combination, correct values can be computed for ‘offset’ and ‘aoffset’. Applying the deblending procedure to each of the 56 source-line files should yield 56 files containing source-receiver-line gathers, a conventional 3D data arrangement. The files can then be appended to one another to create the complete 3D survey, prior to applying 3D geometry and binning the data for imaging.

An additional consideration for these data is that care must be taken not to alter the relative amplitudes of reflections during the deblending process. Since the wavefield separation method we use (RT filtering) only subtracts unwanted events and does not

alter the amplitude of underlying reflections (Henley and Wong, 2011b), in order to preserve reflection amplitudes for AVAZ analysis, it should only be necessary to ensure that no ensemble normalization is applied at any point to the various trace gathers, unless it is later reversed.

Imaging

As a further verification of our deblending process, we display some CMP stacks assembled from the deblended portion of the 3D puck and channel survey. Due to the asymmetry of the subsurface coverage of the part of the survey we processed, we did not attempt to apply 3D geometry or to bin the traces for proper 3D subsurface imaging. Instead, we opted to form quasi-2D CMP stacks from selected subsets of our deblended data. The easiest of these subsets to construct and visualize are 2D broadside CMP stacks, constructed from the data recorded from all the sources on a source line into all the receivers on a selected parallel receiver line. Figure 22 is a schematic showing the subsurface raypath geometry for such a quasi-2D CMP stack. For receiver line 1, parallel to the source line and closest to it, the 'broadside stack' is very similar to a conventional 2D CMP stack; but for receiver lines separated further from the source line, the resulting CMP stacks are more properly 'broadside stacks'. Figures 23, 24, 25, and 26 are examples of broadside CMP stacks corresponding to receiver lines 1, 10, 20, and 30, respectively. Since receiver line 30 is located near the centre of the physical model, the corresponding CMP coverage lies along a line parallel to the source and receiver lines and midway between the centreline of the model and its edge. The other quasi-2D CMP stacks correspond to lines even closer to the model edge. This means that the subsurface illumination of the physical model from this portion of the complete 3D survey is quite limited. Indeed, it can be seen that the reflection marking the bottom of the model at 1400ms can be seen clearly on the stack for receiver line 30, but that shallower reflections are much weaker, due to the oblique raypath angles caused by the offset of source line from receiver line. The top surface of the model at 400ms can most clearly be seen in the two nearest broadside CMP stacks, but deeper reflections are less distinct.

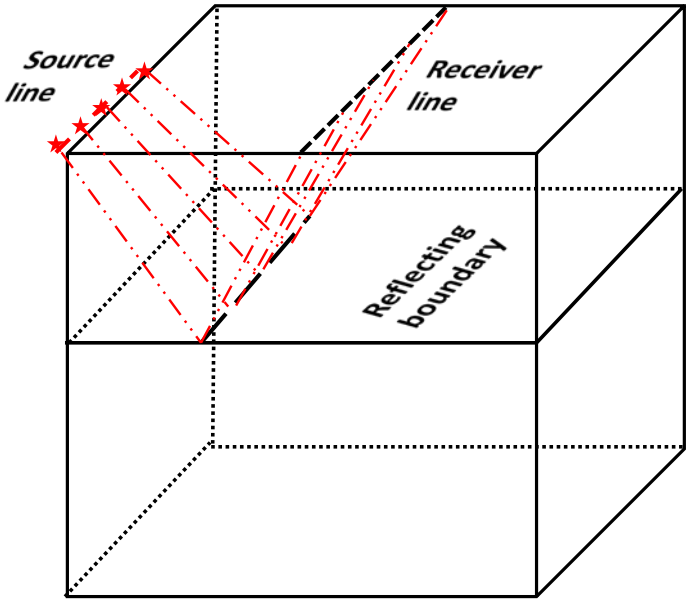

Geometry for a broadside stack showing selected raypaths

FIG. 22. Schematic showing the source and receiver geometry and selected raypaths for the so-called 'broadside CMP stack', of which the 'inline stack' is a special case.

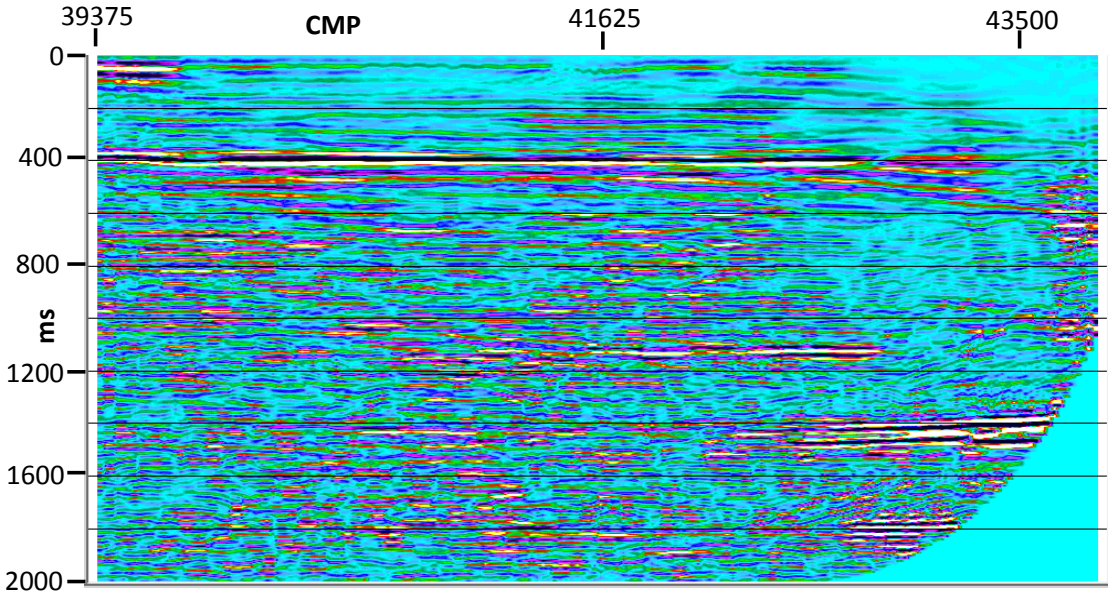

FIG. 23. Broadside CMP stack for source line 1 and receiver line 1; the 'inline stack'.

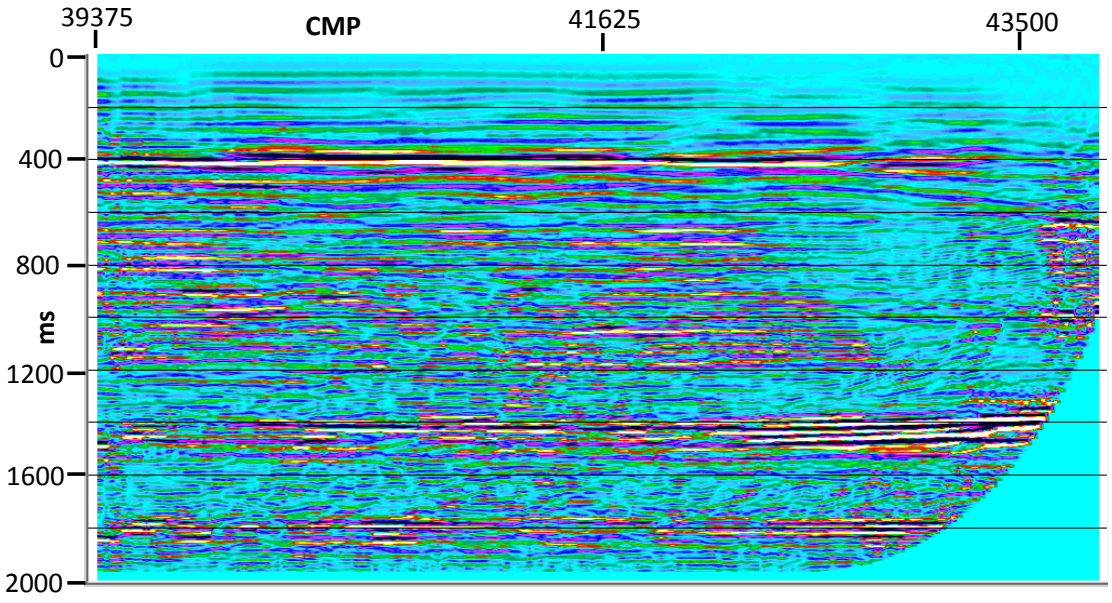

FIG. 24. Broadside CMP stack for source line 1 and receiver line 10.

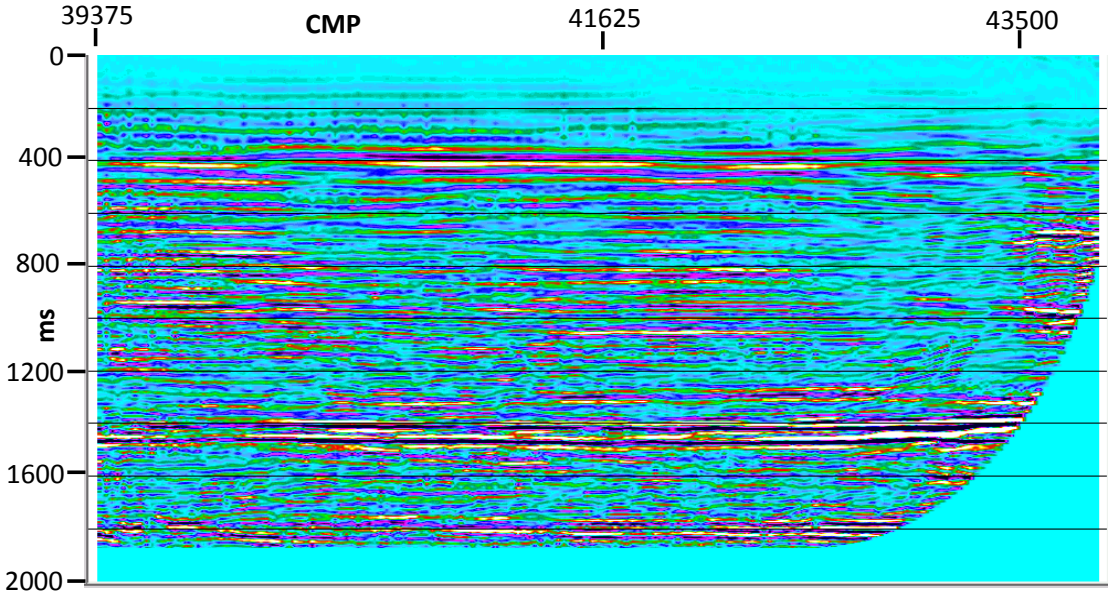

FIG. 25. Broadside CMP stack for source line 1 and receiver line 20.

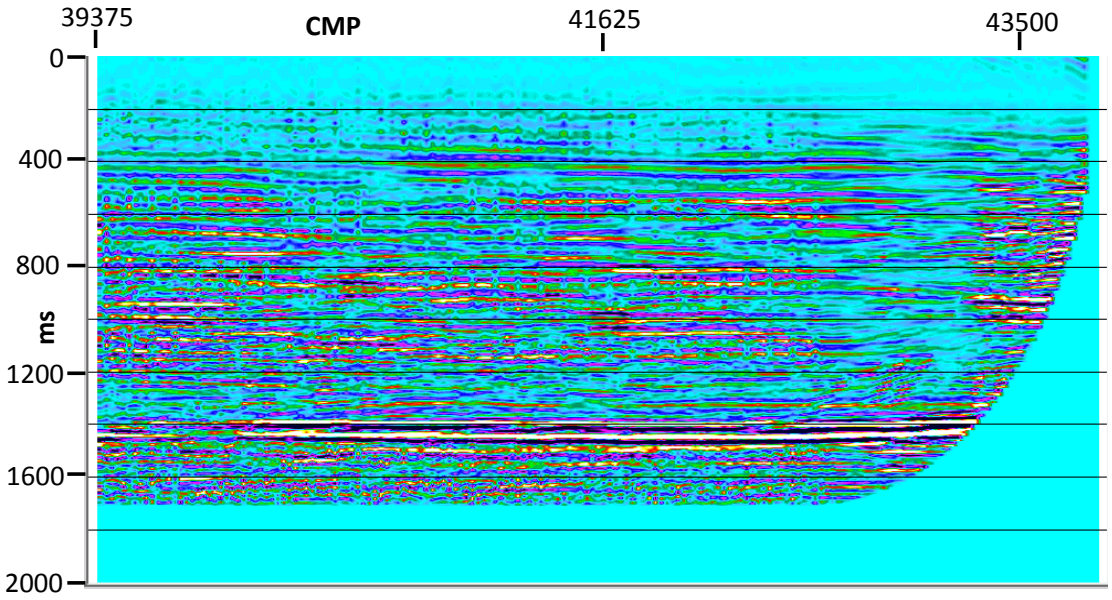

FIG. 26. Broadside CMP stack for source line 1 and receiver line 30.

Another quasi-2D CMP stack configuration that we display here is what we have termed the 2.5D CMP cross-stack. These stacks are parallel to crosslines and are constructed by stacking limited-offset CMP gathers centered on selected crosslines. Figure 27 shows the geometry for such stacks schematically, and Figures 28, 29, and 30 are examples of 2.5D CMP cross-stacks corresponding to crosslines 1-3, 28-30, and 58-60, respectively.

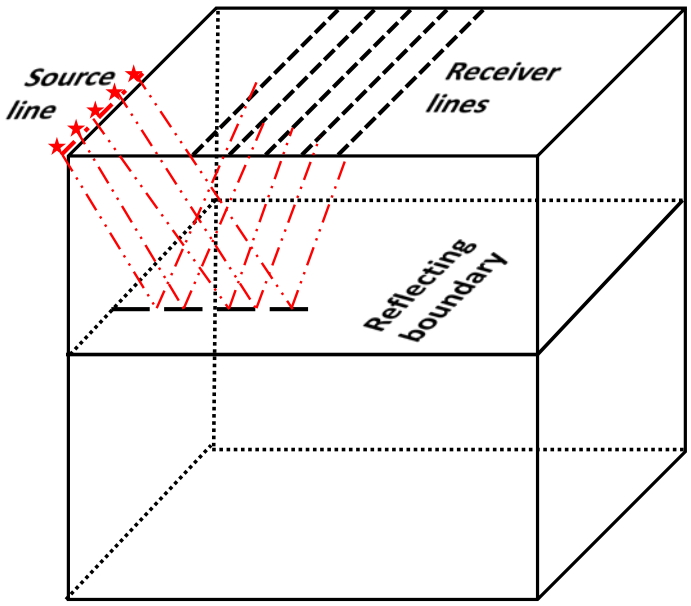

FIG. 27. Schematic showing the source and receiver geometry and selected raypaths for the 2.5D CMP cross-stack.

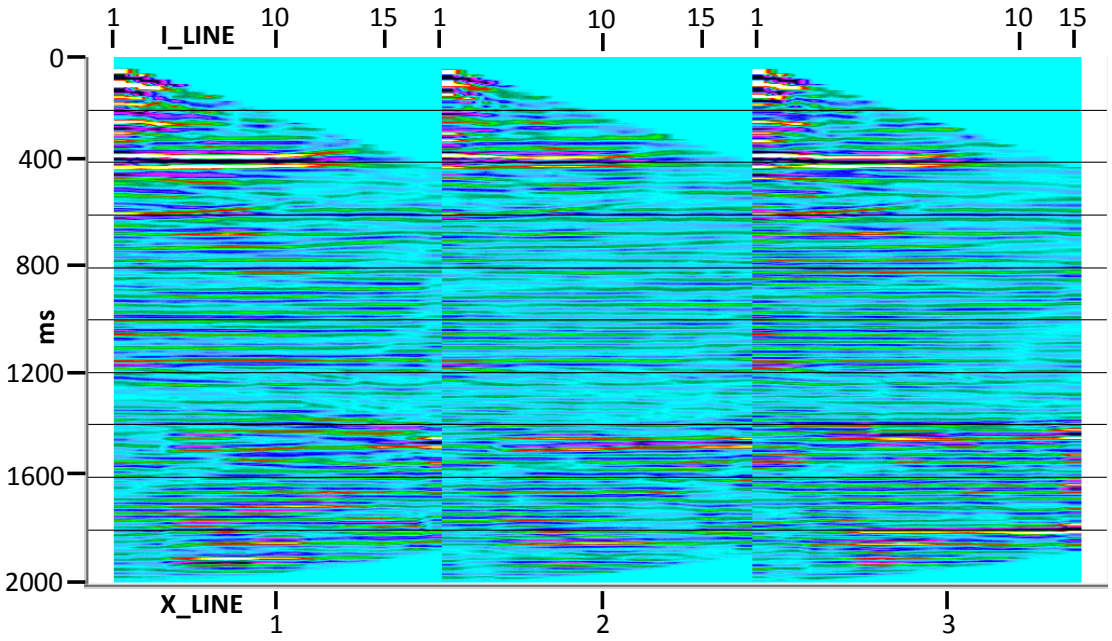

FIG. 28. 2.5D CMP cross-stacks for cross-lines 1, 2, and 3.

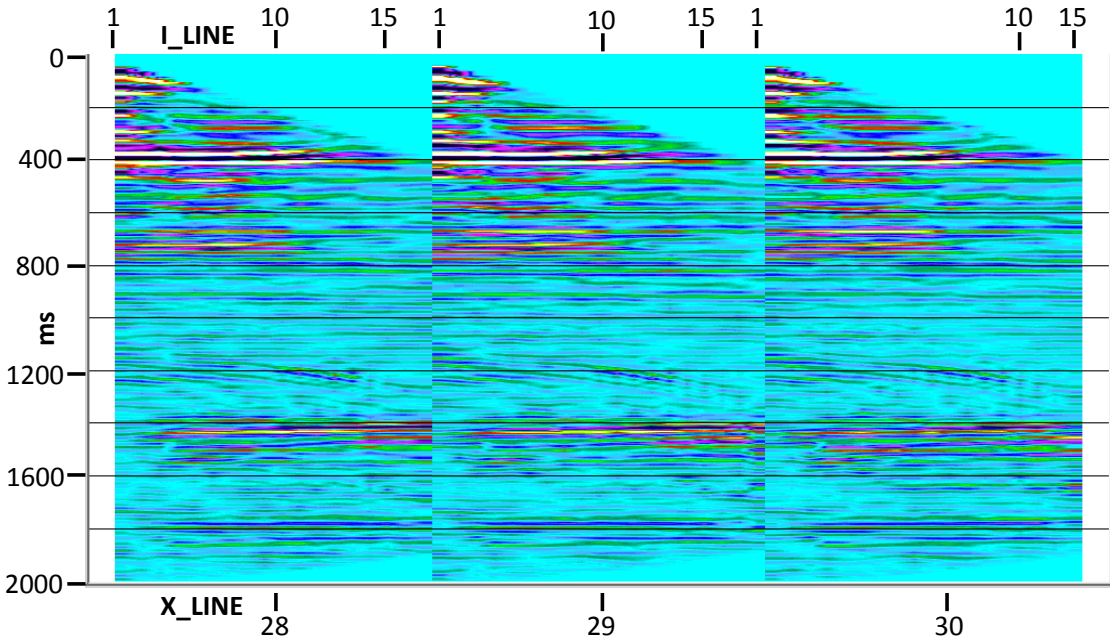

FIG. 29. 2.5D CMP cross-stacks for cross-lines 28, 29, and 30.

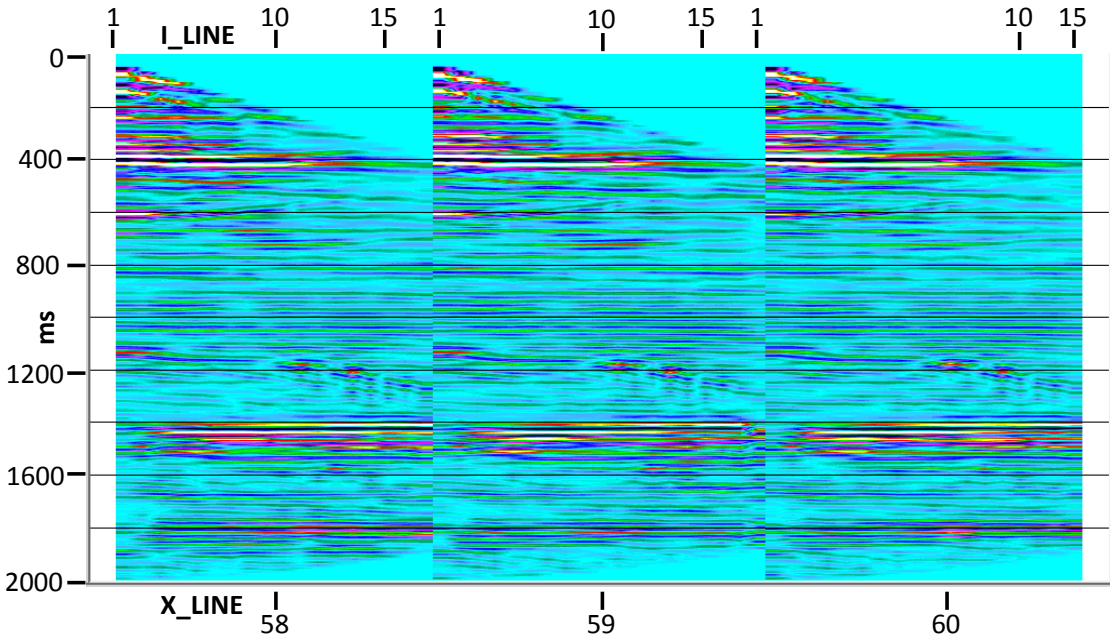

FIG. 30. 2.5D CMP cross-stacks for cross-lines 58, 59, and 60.

Because of the subsurface coverage limitations implied by the restrictions of source locations to half of one edge of the physical model, the quasi-2D broadside stacks and cross-stacks cannot be compared meaningfully to true 3D inline stacks or crossline stacks. Nevertheless, we can use them to help judge the quality of our deblending process as applied to this fragment of a full 3D survey, mainly by examining them for any artifacts indicating wavefield leakage from simultaneous sources.

COMMENTS

We have demonstrated a deblending method, based on previously-described wavefield separation techniques, on a small portion of a large 3D physical model seismic survey. While the portion of the total model processed was too near the edge to consider 3D imaging, or any attempt to detect the known anomalies in the model, our quasi-2D broadside stacks and cross-stacks were free of any visible artifacts due to incomplete deblending. We anticipate using the method to deblend the entire 3D data set for further analysis by CREWES staff and students in the future.

While the receiver spacing used in the survey was too sparse to prevent spatial aliasing of some of the events on the supergathers, our deblending method, because it differentially stretches the time axis of the data, removes most of the visible aliasing before estimating and subtracting interference from neighboring shots.

If more sources were available, there is no reason why they could not be deployed along the entire length of the source line, as long as the source separation was at least 4 source stations. This would cut acquisition time by a further factor of 2, with no effect on the data quality.

ACKNOWLEDGEMENTS

The authors acknowledge the funding of CREWES sponsors and NSERC, and the support of sponsors and staff.

REFERENCES

Beasley, C., 2008, A new look at marine simultaneous sources, The Leading Edge, **27**, 914-917.

Cheng, J., and Sacchi, M., 2013, Separation of simultaneous source data via iterative rank reduction, SEG Technical Progarm Expanded Abstracts, pp. 88-93 doi: 10.1190/segam2013-1313.1

Henley, D.C., 2003, Coherent noise attenuation in the radial trace domain, Geophysics, **68**, No. 4, P1408-1416.

Henley, D.C., and Wong, J, 2011a, Getting something for nothing--or not: interpolating coherent noise, CREWES Research Report **23** (2011).

Henley, D.C., and Wong, J., 2011b, How processing affects relative reflection amplitudes, CREWES Research Report **23** (2011).

Henley, D.C. and Wong, J., 2013a, Through the looking glass: using X-T plane distortions for wavefield separation, CREWES Research Report **25**.

Henley., D.C., and Mahmoudian, F., 2013b, Undoing wavefield interference for AVAZ measurements, CREWES Research Report **25**.

Trad, D., Siliqi, R., Poole, G., and Boelle, J., 2012, Fast and robust deblending using Apex Shifted Radon Transform, SEG Technical Program Expanded Abstracts, pp 1-5, doi: 10.1190/segam2012-0703.1

Wong, J, 2013, Seismic physical modeling I: Acquisition of 2D and 3D surveys involving HTI targets, CREWES Research Report **25** (2013).

Wong, J., 2013, Seismic physical modeling II: VVAZ and AVAZ effects observed on reflections from isolated HTI targets, CREWES Research Report **25** (2013).